Available online at www.sciencedirect.com
ScienceDirect
Trans. Nonferrous Met. Soc. China 27(2017) 1127−1133
Transactions of Nonferrous Metals Society of China
www.tnmsc.cn

Photochemical synthesis and enhanced photocatalytic activity of $MnO_x/BiPO_4$ heterojunction

Hai-bin LI, Guo-you HUANG, Jian ZHANG, Sheng-hao FU, Teng-gan WANG, Hong-wei LIAO

School of Materials Science and Engineering,
Changsha University of Science and Technology, Changsha 410114, China

Received 4 April 2016; accepted 18 December 2016

Abstract: Monoclinic $BiPO_4$ with rod-like shape was prepared via a CTAB-assisted hydrothermal route. MnO_x nanoparticles were loaded on the surfaces of $BiPO_4$ rods by a photo-deposition process to form $MnO_x/BiPO_4$ heterojunctions. The as-prepared samples were characterized by XRD, SEM, TEM, XPS, FL, and UV-Vis diffuse reflectance measurements. The results showed that MnO_x nanoparticles were strongly anchored to the surfaces of $BiPO_4$ rods when the mole ratio of Mn to Bi was controlled at a low level, forming $MnO_x/BiPO_4$ heterojunctions with effective and sound interfaces. The $MnO_x/BiPO_4$ heterojunctions exhibited higher photoactivity than pristine $BiPO_4$ for photodegradation of methyl blue under UV irradiation, which could be attributed to the efficient charge transfer at the heterojunction interfaces. The higher light absorption ability of $MnO_x/BiPO_4$ in the range of 300−420 nm compared with pristine $BiPO_4$ was also responsible for the enhanced photocatalytic activities of $MnO_x/BiPO_4$ heterojunctions.
Key words: $BiPO_4$; photocatalysis; hydrothermal method; MnO_x; heterojunction; photodeposition

1 Introduction

Semiconductor photocatalysis is expected to be a very promising technology to address problems in environmental remediation and energy utilization [1,2]. Recently, many Bi-based semiconductors, such as $BiVO_4$ [3], Bi_2MoO_6 [4], $BiWO_6$ [5,6], and $BiPO_4$ [7], have been applied as photocatalysts. Among these photocatalysts, $BiPO_4$ has attracted more and more attention. $BiPO_4$ mainly exists in three crystalline phases: monoclinic structure, monoclinic monazite structure, and hexagonal structure. Among them, the monoclinic $BiPO_4$ shows the best photocatalytic activity due to its high photocatalytic activity, excellent absorption of UV, strong oxidation ability and chemical stability in aqueous solution, while that of the hexagonal $BiPO_4$ is the worst [7]. It was reported that the photocatalytic activity of monoclinic $BiPO_4$ is much better than that of Degussa P25 TiO_2 [8]. However, monoclinic $BiPO_4$ still suffers from its wide bandgap (4.2 eV), poor adsorptive performance, and large size [9], which limits the utilization of visible light and the separation of photoinduced charge carriers, hindering further improvement of photocatalytic activity. Therefore, it is highly necessary to develop an effective method to solve those problems.

Combining with a cocatalyst, such as a noble metal or another semiconductor, to form heterojunction is an effective way to broaden the light absorption range and promote the separation of photoinduced charge carriers of a photocatalyst. Noble metals, such as Ag, Pt, and Au, are deriving-electron type cocatalysts, while some semiconductors, such as MnO_x, PbO_x, and Ag_3PO_4, are deriving-hole-type cocatalysts [9−11]. It was reported that both Ag and Ag_3PO_4 could enhance the separation efficiency of the photoinduced holes and electrons of $BiPO_4$, improving the photocatalytic activity [11,12]. MnO_x is a photocatalyst with high activity owe to its small particle size, strong adsorptivity, and excellent absorption of visible light [10]. So, anchoring MnO_x on the surface of $BiPO_4$ to form a stable heterojunction may cover the shortage of $BiPO_4$. In addition, photo-induced holes are the main active species of $BiPO_4$ for dye degradation [10]. Therefore, deriving-hole-type MnO_x may effectively improve the separation efficiency of the

Foundation item: Project (51102025) supported by the National Natural Science Foundation of China; Project (14JJ7040) supported by Natural Science Foundation of Hunan Province, China; Project (2014GH561172) supported by China Torch Program
Corresponding author: Hai-bin LI; Tel:+86-731-85258232; Fax: +86-731-82309128; E-mail: coastllee@hotmail.com
DOI: 10.1016/S1003-6326(17)60131-6

photoinduced charge carriers of $BiPO_4$. However, to our best knowledge, there are no reports about deposition of MnO_x on $BiPO_4$.

Herein, monoclinic $BiPO_4$ rods were prepared via a hydrothermal approach, MnO_x nanoparticles were then loaded on the surface of $BiPO_4$ rods by a photo-deposition process to form a novel $MnO_x/BiPO_4$ heterojunctions. The photoactivities of the as-prepared samples were evaluated by degradation of methyl blue (MB) under UV irradiation.

2 Experimental

2.1 Preparation of $BiPO_4$

All reagents were of AR grades and used without further purification. Deionized water was used in all experiments. $BiPO_4$ was synthesized as follows: 1.15 g of $Na_3PO_4·12H_2O$ and 0.25 g of CTAB were dissolved into 15 mL of deionized water, while 1.46 g of $Bi(NO_3)_3·5H_2O$ was dissolved into 15 mL of HNO_3 solution (1 mol/L). The two solutions were then mixed up. NaOH solution (2 mol/L) was dropwise added to tailor the pH of the mixture under magnetic stirring. The obtained suspension was fixed to 40 mL by adding deionized water. After being stirred for 30 min, the suspension was transferred into a 50 mL Teflon-lined autoclave stainless steel autoclave. The autoclave was heated at 140 °C for 15 h, and then cooled to room temperature naturally. The product was collected, washed with deionized water and absolute alcohol three times, respectively, and finally dried at 80 °C for 20 h to obtain $BiPO_4$ powders.

2.2 Preparation of $MnO_x/BiPO_4$ heterojunctions

$MnO_x/BiPO_4$ heterojunctions were synthesized by photo-deposition. 1 g of $BiPO_4$ was ultrasonically dispersed into 100 mL deionized water, then a certain amount of $MnSO_4·H_2O$ was dissolved into the suspension (the mole ratios of Mn to Bi were controlled at 0.05, 0.08, and 0.15, respectively). The mixture was magnetically stirred for 24 h in the dark, and then irradiated for 3 h under UV light. The product was collected and thoroughly washed with deionized water and ethanol respectively, and finally dried at 80 °C for 20 h to obtain $MnO_x/BiPO_4$ heterojunctions. The as-prepared samples were characterized and confirmed for the Mn to Bi mole ratio via atomic absorption spectroscopy (AAS) using Chem. Tech Analytical 2000 spectrophotometer.

2.3 Characterization

The crystalline structure of the sample was analyzed by a Rigaku D/Max 2500 powder diffractometer (XRD) with Cu K_α radiation (λ=1.5406 Å). The morphology of the as-prepared samples was investigated by transmission electron microscopy (TEM, Philips Tecnai20G2S-TWIN) and environmental scanning electron microscope (ESEM, FEI QUANTA 250). X-ray photoelectron spectroscopy (XPS) data of the samples were determined with a K-Alpha 1063 electron spectrometer from Thermo Fisher Scientific using 72 W Al K_α radiation. UV-Vis diffuse reflectance spectra were measured with a Specord 200 UV spectrophotometer. Photoluminescence spectroscopy analysis (PL) of the samples was carried out on a Hitachi F−4500 fluorescence spectrophotometer.

2.4 Photocatalytic test

The photocatalytic properties of $MnO_x/BiPO_4$ heterojunctions were assessed by photodegradation of MB aqueous solution under ultraviolet irradiation with a 45 W ultraviolet lamp. 0.2 g of photocatalyst was mixed with 100 mL of 10 mg/L methyl orange aqueous solution. The mixture was ultrasonically dispersed for 10 min and then magnetically stirred in dark for 30 min before commencing the photocatalytic reactions to allow the system to reach an adsorption/desorption equilibrium. All photocatalytic reactions were carried out in a laboratory constructed photoreactor. 3 mL of sample solution was taken at given time intervals and separated through centrifugation. The concentrations of MB solution were evaluated by an UNICO UV−2100 spectrophotometer at 660 nm.

3 Results and discussion

3.1 Structure and morphology of $BiPO_4$

Figure 1 shows the XRD patterns of the products prepared at different pH values. It can be found that all the diffraction peaks of the samples prepared at pH 1 and 2 are readily indexed to a pure phase of monoclinic $BiPO_4$ (JCPDS No. 15−0767), while those of the sample prepared at pH 4 are indexed to a pure phase of hexagonal $BiPO_4$ (JCPDS No. 45−1370). The strong and sharp diffraction peaks indicate that these three samples are highly crystalline. When the pH is tailored to 6, the characteristic diffraction peaks corresponding to both monoclinic $BiPO_4$ and hexagonal $BiPO_4$ are found in the XRD pattern, indicating the coexistence of monoclinic $BiPO_4$ and hexagonal $BiPO_4$. Moreover, the diffraction peak intensity decreases obviously compared with that of the other samples. It can be deduced that pH plays a key role in the crystal phases of the products in the present case, and strong acid condition favors the growth of monoclinic $BiPO_4$, which was reported to show the highest photocatalytic activity among the three crystalline phases of $BiPO_4$ [7].

Figures 2(a) and (b) show the SEM images of the

monoclinic $BiPO_4$ prepared at pH 1 and 2, respectively. It can be clearly seen that both samples consist of rod-like particles with lengths of 1−2 μm and diameters of 100−400 nm. The smooth surfaces indicate the high crystallinity of the products, which is consistent with the XRD results.

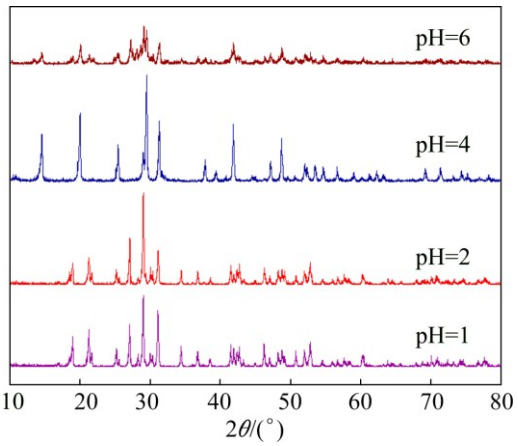

Fig. 1 XRD patterns of samples prepared at different pH

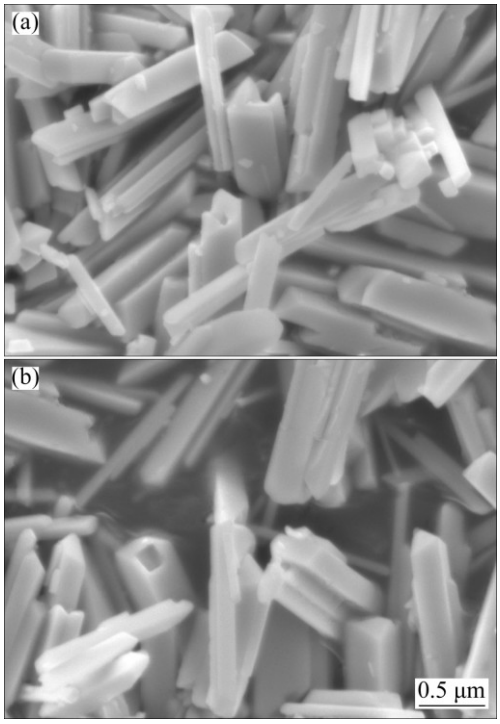

Fig. 2 SEM images of monoclinic $BiPO_4$ prepared at pH=1 (a) and pH=2 (b)

3.2 Structure and morphology of $MnO_x/BiPO_4$ heterojunctions

$MnO_x/BiPO_4$ heterojunctions were obtained by photodeposition of MnO_x on the surface of monoclinic $BiPO_4$ rods prepared at pH 2. Figure 3 shows the XRD patterns of $MnO_x/BiPO_4$ heterojunctions with different mole ratios of Mn to Bi. It can be seen that for all the samples, only characteristic peaks corresponding to monoclinic $BiPO_4$ (JCPDS No. 15−0767) are found, no characteristic peaks resulted from manganese oxide can be seen even though the Mn to Bi mole ratio of the heaviest MnO_x-loaded $BiPO_4$ is 0.15:1. Since MnO_x was prepared by photodeposition of Mn^{2+} from $MnSO_4$ aqueous solution without calcination, it is most likely that the obtained MnO_x is amorphous, resulting in the disappearance of the characteristic diffraction peaks of MnO_x.

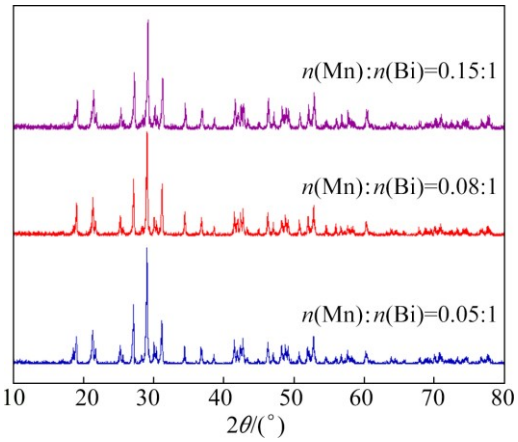

Fig. 3 XRD patterns of $MnO_x/BiPO_4$ with different mole ratios of Mn to Bi

The microstructures of $MnO_x/BiPO_4$ heterojunctions were investigated by TEM and HRTEM. As shown in Fig. 4(a), the sample with a Mn to Bi mole ratio of 0.08:1 consists of rod-like $BiPO_4$ with plenty of MnO_x nanoparticles strongly anchored on the surfaces. The insert shows the HRTEM image corresponding to the marked area. The lattice structure of $BiPO_4$ is very orderly and different from that of MnO_x nanoparticles. The lattice spacing of 0.327 nm is assigned to the interplanar spacing of monoclinic $BiPO_4$ (200) plane. The lattice structure of MnO_x is rather indistinct, which may be attributed to its amorphism. The obvious interfaces between $BiPO_4$ rod and MnO_x nanoparticles shown in HRTEM image suggest the formation of well-defined heterojunction structures of $MnO_x/BiPO_4$ composites, which is beneficial to the charge carrier separation at the interfaces, improving the quantum yield of the photocatalyst. However, MnO_x particles are not found on the surfaces of $BiPO_4$ rods when the Mn to Bi mole ratio is increased to 0.15:1, but scatter around the $BiPO_4$ rods, indicating that $MnO_x/BiPO_4$ heterojunctions are not formed under this condition. We consider the formation of $MnO_x/BiPO_4$ heterojunctions is mainly due to the heterogeneous nucleation of MnO_x on the surfaces of rod-like $BiPO_4$ when the concentration of Mn^{2+} in the suspension is very low. The similar process for constructing Ag/TiO_2 nanotube heterojunctions has been demonstrated in our previous work [13]. As the

concentration of Mn^{2+} increased to a relatively high level (Mn to Bi mole ratio of 0.15:1), homogeneous nucleation of MnO_x in the suspension dominates, forming scattered MnO_x particles around rod-like $BiPO_4$.

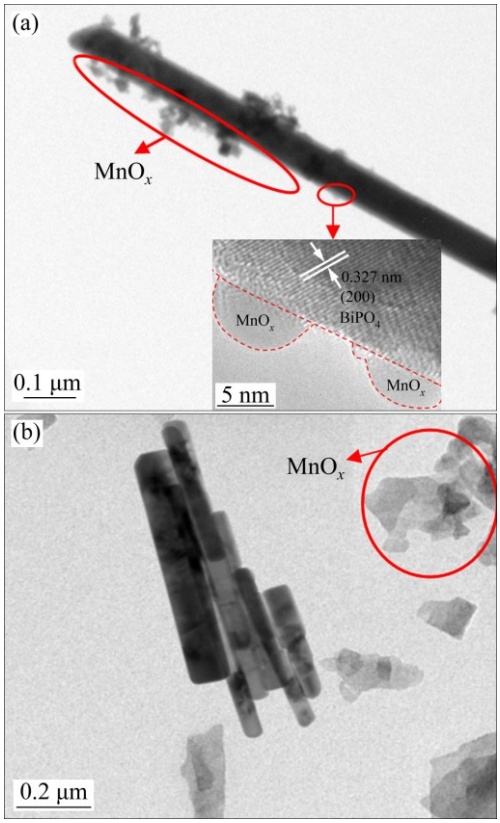

Fig. 4 TEM images of $MnO_x/BiPO_4$ heterojunction with Mn to Bi mole ratio of 0.08:1 (a) and TEM image of $MnO_x/BiPO_4$ with Mn to Bi mole ratio of 0.15:1 (b) (Insert is HRTEM image of marked area)

Figure 5 shows the high-resolution XPS spectra of the Bi 4f, P 2p, and Mn 2p for $MnO_x/BiPO_4$ with a Mn to Bi mole ratio of 0.08:1. As shown in Fig. 5(a), the two peaks at 158.9 and 164.2 eV are attributed to the Bi $4f_{7/2}$ and Bi $4f_{5/2}$ of Bi^{3+} in $BiPO_4$, respectively [10,14]. The P 2p XPS peak can be found at 132.9 eV (Fig. 5(b)), and the peak is ascribed to the P^{5+} in $BiPO_4$ [14]. Figure 5(c) shows the Mn 2p XPS spectrum. The binding energies of Mn $2p_{3/2}$ for the manganese cations in MnO, Mn_2O_3, and MnO_2 were reported at 640.9, 641.8, and 642.4 eV, respectively [15]. Based on the above fact, the Mn $2p_{3/2}$ peak in Fig. 5(c) is fitted by the Gauss−Lorentz method. Three peaks at 640.5, 641.6, and 643.0 eV are obtained, which correspond to Mn^{2+}, Mn^{3+} and Mn^{4+} in the $MnO_x/BiPO_4$ heterojunctions, respectively. And the main states of manganese in $MnO_x/BiPO_4$ are Mn^{3+} and Mn^{4+}.

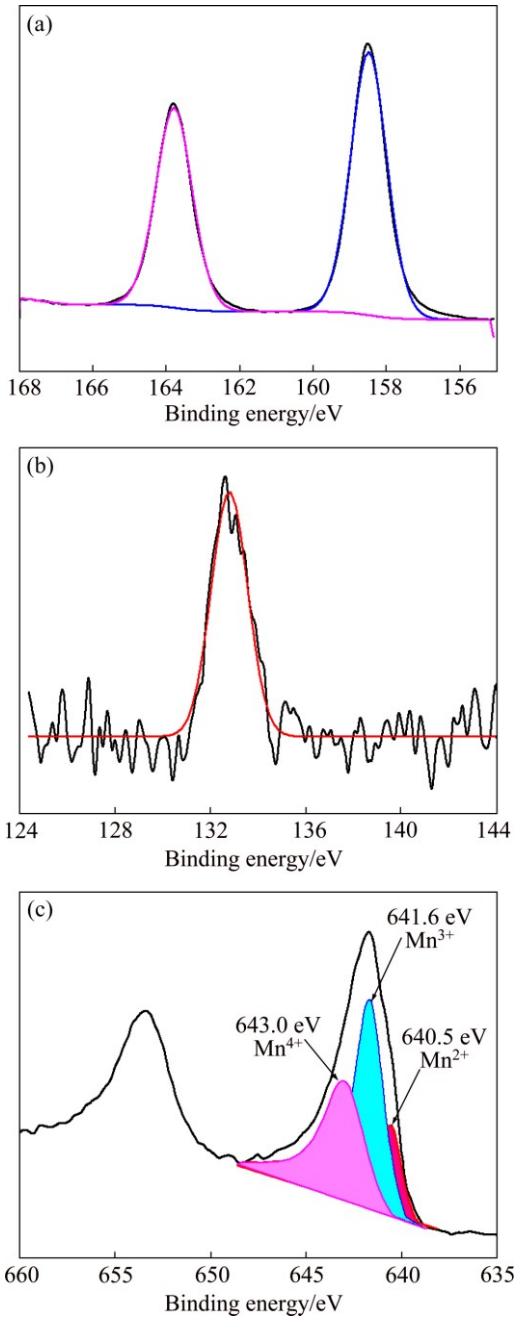

Fig. 5 High resolution XPS spectra of Bi 4f (a), P 2p (b), and Mn 2p (c) for $MnO_x/BiPO_4$ heterojunction with Mn to Bi mole ratio of 0.08:1

3.3 UV-Vis analysis

Figure 6 shows the UV-Vis diffuse reflectance spectra of the pristine $BiPO_4$ and $MnO_x/BiPO_4$ heterojunctions with Mn to Bi mole ratios of 0.08:1 and 0.15:1. The pristine $BiPO_4$ shows strong absorption in the UV range with absorption edge at about 290 nm. The spectrum is steep, indicating that the UV light absorption is resulted from the band-gap transition. The band-gap energy was calculated to be 4.2 eV, according to the formula $\lambda_g=1239.8/E_g$, where λ_g is the band-gap wavelength, E_g is the bandgap energy, which is in good agreement with those reported in previous works [16]. For the $MnO_x/BiPO_4$ heterojunctions, the absorption

intensities in the range of 300−420 nm are significantly enhanced compared with that of pristine $BiPO_4$, which is ascribed to the loading of MnO_x with narrow bandgap on the surface of $BiPO_4$ rods, indicating that coupling with MnO_x may broaden the light absorption range of the photocatalyst and cover the shortage of $BiPO_4$.

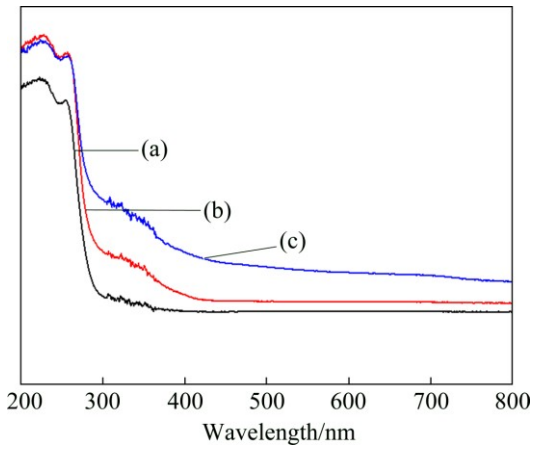

Fig. 6 UV-Vis diffuse reflectance spectra of pristine $BiPO_4$ (a) and $MnO_x/BiPO_4$ heterojunctions with different Mn to Bi mole ratios of 0.08:1 (b) and 0.15:1 (c)

3.4 Photocatalytic activity of $MnO_x/BiPO_4$ heterojunction

The effects of MnO_x deposition on the photocatalytic activity of $BiPO_4$ were evaluated by measuring the degradation of MB in aqueous solution under UV irradiation. Figure 7 shows the photodegradation efficiencies of MB as a function of irradiation time by the pristine $BiPO_4$ and $MnO_x/BiPO_4$ heterojunctions with different Mn to Bi mole ratios. After 30 min of UV irradiation, MB removals by the pristine $BiPO_4$ and $MnO_x/BiPO_4$ heterojunctions with Mn to Bi mole ratios of 0.05:1, 0.08:1, and 0.15:1 are 49%, 77%, 92%, and 61%, respectively. The time for complete decomposition of MB by the pristine $BiPO_4$ and

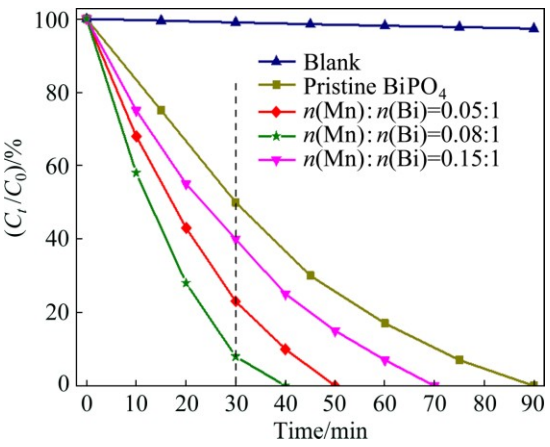

Fig. 7 Photocatalytic degradation efficiency of MB by pristine $BiPO_4$ and $MnO_x/BiPO_4$ with different Mn to Bi mole ratios

$MnO_x/BiPO_4$ heterojunctions with Mn to Bi mole ratios of 0.05:1, 0.08:1, and 0.15:1 is 90, 50, 40, and 70 min, respectively. These results suggest that coupling $BiPO_4$ with MnO_x can effectively improve the photocatalytic efficiency of $BiPO_4$, and there is an optimum value for MnO_x loading. Further increasing the loading amount of MnO_x beyond this level shows detrimental effects on the photodegradation of MB.

To further understand the the photocatalytic efficiency of the above samples, the plot of $\ln(C_t/C_0)$ as a function of time is shown in Fig. 8, where C_0 and C_t are the concentrations of methyl orange in the primary stage of experimental and after UV irradiation [17]. It can be seen that the variation of $\ln(C_t/C_0)$ with time follows a linear trend in all the plots. The photocatalytic reaction rate constant k can be calculated according to the following formula: $\ln(C_t/C_0)=-kt$ [17]. For the pristine $BiPO_4$ and $MnO_x/BiPO_4$ heterojunctions with Mn to Bi mole ratios of 0.05:1, 0.08:1, and 0.15:1, the k values were found to be 0.037, 0.060, 0.079, 0.044 min^{-1}, respectively.

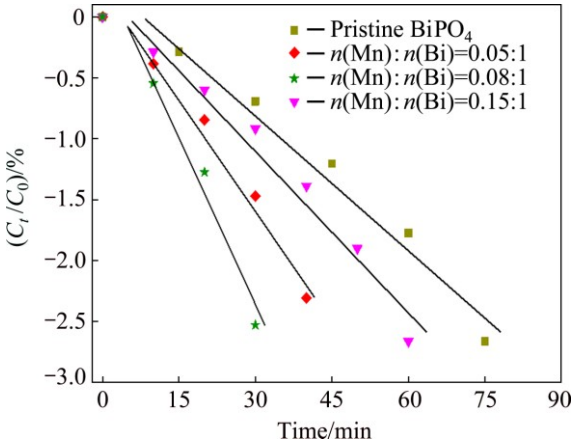

Fig. 8 Kinetics of degradation of MB by pristine $BiPO_4$ and $MnO_x/BiPO_4$ with different Mn to Bi mole ratios

The previous works revealed that the surface area, photoabsorption ability, and the separation and transporting rate of photogenerated electrons and holes are the main factors that affect the catalytic activity of a photocatalyst [18]. Since the pristine $BiPO_4$ and $MnO_x/BiPO_4$ heterojunctions possess similar morphology, the photocatalytic activity enhancement of $MnO_x/BiPO_4$ heterojunctions could be mainly attributed to the efficient charge separation and high transporting rate of photogenerated electrons and holes. Figure 9 presents the PL spectra of the pristine $BiPO_4$ and $MnO_x/BiPO_4$ heterojunctions with different Mn to Bi mole ratios of 0.05:1, 0.08:1 and 0.15:1. Photoluminescence is resulted from the recombination of photo-generated electrons and holes. The higher intensity of PL spectrum indicates the higher rate of recombination. Therefore, PL spectrum is

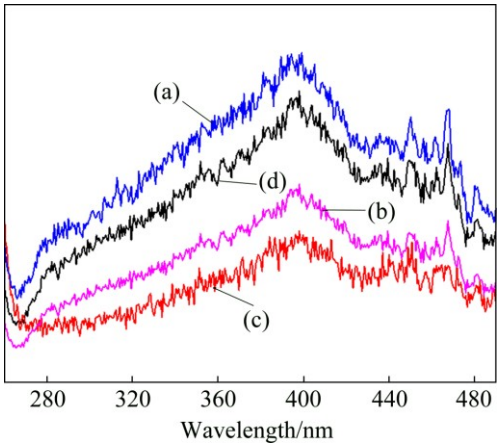

Fig. 9 PL spectra of pristine $BiPO_4$ (a) and $MnO_x/BiPO_4$ heterojunctions with different Mn to Bi mole ratios of 0.05:1 (b), 0.08:1 (c) and 0.15:1 (d)

usually applied to investigating the efficiency of charge carrier transfer, migration and separation [19,20]. It can be clearly seen that the PL intensity of $MnO_x/BiPO_4$ heterojunction first decreases with increasing the Mn to Bi mole ratio and reaches the lowest value when Mn to Bi mole ratio is 0.08:1. Further increase of Mn to Bi mole ratio of 0.15:1 leads to a rise in PL intensity. This reveals that coupling a suitable amount of MnO_x with $BiPO_4$ can effectively enhance the charge carrier separation of $BiPO_4$. Both $BiPO_4$ and MnO_x are semiconductor oxides, so a heterojunction will be formed at the interfaces between $BiPO_4$ and MnO_x when they are closely joined together, and an internal field will emerge due to the potential of band energy difference [9,10]. MnO_x is a deriving-hole-type cocatalyst, the photoinduced holes in the valence band of $BiPO_4$ may transfer to that of MnO_x due to the internal field at the interfaces. Such electric- field- assisted charge transfer at the heterojunction interfaces promotes the separation efficiency of photo-generated electron–holes and improves the quantum yield, leading to the photocatalytic efficiency enhancement of $MnO_x/BiPO_4$ composites [11,18,20,21]. The higher photoabsorption ability of $MnO_x/BiPO_4$ in the range of 300−420 nm compared with pristine $BiPO_4$, which is revealed by the UV-Vis diffuse reflectance spectra (Fig. 6), is also responsible for the enhanced photocatalytic activity of $MnO_x/BiPO_4$ heterojunctions. It should be noted that the excess coupled content of MnO_x (Mn to Bi mole ratio of 0.15:1) may result in the scattering of MnO_x particles and the damage of the interfaces between MnO_x and $BiPO_4$, as observed in Fig. 4(b), which is unfavorable for the charge carrier transfer between MnO_x and $BiPO_4$, resulting in a low quantum yield and a weak photocatalytic performance compared with that of $MnO_x/BiPO_4$ with a Mn to Bi mole ratio of 0.08:1.

Figure 10 presents the results of repeating experiments on photodegradation of MB by $MnO_x/BiPO_4$ heterojunctions with a Mn to Bi mole ratio of 0.08:1. After each run, the photocatalysts were collected by centrifugation followed by ultrasonic cleaning with distilled water. As shown in Fig. 10, no significant loss is found after five successive cycles, suggesting that the sample is stable and not photocorroded in the photocatalytic reactions.

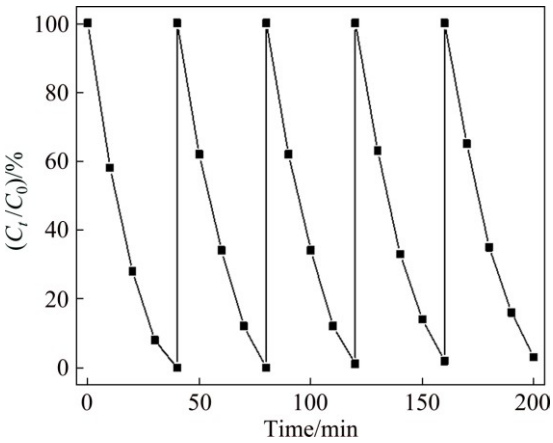

Fig. 10 Cyclic photodegradation curve for $MnO_x/BiPO_4$ heterojunctions with Mn to Bi mole ratio of 0.08:1

4 Conclusions

1) The $MnO_x/BiPO_4$ heterojunctions were successfully synthesized by the photodeposition of MnO_x on the surfaces of hydrothermally prepared monoclinic $BiPO_4$ rods.

2) The $MnO_x/BiPO_4$ heterojunctions with a suitable Mn to Bi mole ratio exhibited higher photocatalytic activities than the pristine $BiPO_4$ for the degradation of MB under UV irradiation.

3) The TEM and PL studies reveal that the effective and sound interfaces of the $MnO_x/BiPO_4$ heterojunctions play a key role in the efficient separation of electrons and holes for the enhancement of photocatalytic activity. The higher light absorption ability of $MnO_x/BiPO_4$ in the range of 300−420 nm compared with pristine $BiPO_4$ is also helpful to enhancing the photocatalytic activities of $MnO_x/BiPO_4$ heterojunctions.

References

[1] YANG Xi-jia, WANG Shu, SUN Hai-ming, WANG Xiao-bing, LIAN Jian-she. Preparation and photocatalytic performance of Cu-doped TiO_2 nanoparticles [J]. Transactions of Nonferrous Metals Society of China, 2015, 25(2): 504−509.

[2] HUANG Xiao-jun, YAN Xin, WU Hai-yan, FANG Ying, MIN Ya-hong, LI Wen-sheng, WANG Shuang-yin, WU Zhen-jun. Preparation of Zr-doped $CaTiO_3$ with enhanced charge separation efficiency and photocatalytic activity [J]. Transactions of Nonferrous

Metals Society of China, 2016, 26(2): 464−471.
[3] WANG Min, CHE Yin-sheng, NIU Chao, DANG Ming-yan, DONG Duo. Lanthanum and boron co-doped $BiVO_4$ with enhanced visible light photocatalytic activity for degradation of methyl orange [J]. Journal of Rare Earths, 2013, 31(9): 878−884.
[4] UMAPATHY V, MANIKANDAN A, ANTONY S A, RAMU P, NEERAJA P. Structure, morphology and opto-magnetic properties of Bi_2MoO_6 nano-photocatalyst synthesized by sol–gel method [J]. Transactions of Nonferrous Metals Society of China, 2015, 25(10): 3271−3278.
[5] SINGH A, DUTTA D P, ROY M, TYAGI A K, FULEKAR M H. Sonochemical synthesis, characterization, and photocatalytic properties of $Bi_{2-x}Sb_xWO_6$ nanorods [J]. Journal of Materials Science, 2014, 49(5): 2085−2097.
[6] REN Jia, WAN Wen-zhong, SU Song-mei. Enhanced photocatalytic activity of Bi_2WO_6 loaded with Ag nanoparticles under visible light irradiation [J]. Applied Catalysis B: Environmental, 2009, 92(1): 50−55.
[7] ZHU Yan-yan, LING Qiang, LIU Yan-fang, WANG Hua, ZHU Yong-fa. Photocatalytic performance of $BiPO_4$ nanorods adjusted via defects [J]. Applied Catalysis B: Environmental, 2016, 187(15): 204−211.
[8] PAN Cheng-si, ZHU Yong-fa. Size-controlled synthesis of $BiPO_4$ nanocrystals for enhanced photocatalytic performance [J]. Journal of Materials Chemistry, 2011, 21(12): 4235−4241.
[9] LI Ren-gui, ZHANG Fu-xiang, WANG Dong-e, YANG Jing-xiu, LI Ming-run, ZHU Jian, ZHOU Xin, HAN Hong-xian, LI Can. Spatial separation of photogenerated electrons and holes among {010} and {110} crystal facets of $BiVO_4$ [J]. Nature Communications, 2013, 4(2): 66−78.
[10] YE Li-qun, LIU Xiao-di, ZHAO Qiang, XIE Hai-quan, ZAN Ling. Dramatic visible light photocatalytic activity of MnO_x–BiOI heterogeneous photocatalysts and the selectivity of the cocatalyst [J]. Journal of Materials Chemistry A, 2013, 1(31): 431−436.
[11] LIN Hai-li, YE Hui-fang, XU Ben-yan, CAO Jing, CHEN Shi-fu. Ag_3PO_4 quantum dot sensitized $BiPO_4$: A novel p-n junction $Ag_3PO_4/BiPO_4$ with enhanced visible-light photocatalytic activity [J]. Catalysis Communications, 2013, 37(13): 55−59.
[12] ZHANG Yua-nan, FAN Hui-qing, LI Meng-meng, TIAN Hai-lin. Ag/$BiPO_4$ heterostructures: Synthesis, characterization and their enhanced photocatalytic properties [J]. Dalton Transactions, 2013, 42(36): 53−59.
[13] LI Hai-bin, DUAN Xue-chen, LIU Guo-cong, LIU Xiao-qi. Photochemical synthesis and characterization of Ag/TiO_2 nanotube composites [J]. Journal of Materials Science, 2008, 43(5): 1669−1676.
[14] PAN Cheng-si, XU Jing, WANG Ya-jun, LI Di, ZHU Yong-fa. Dramatic activity of $C_3N_4/BiPO_4$ photocatalyst with core/shell structure formed by self-assembly [J]. Advanced Functional Materials, 2012, 22(7): 1518−1524.
[15] ZOU Zhi-Qiang, MENG Ming, ZHA Yu-Qing. Surfactant-assisted synthesis, characterizations, and catalytic oxidation mechanisms of the mesoporous and Pd/MnO_x−CeO_2 catalysts used for CO and C_3H_8 oxidation [J]. The Journal of Physical Chemistry C, 2009, 114(1): 468−477.
[16] OBREGÓN S, ZHANG Yun-fan, COLÓN G. Cascade charge separation mechanism by ternary heterostructured $BiPO_4/TiO_2$/g−C_3N_4 photocatalyst [J]. Applied Catalysis B: Environmental, 2016, 184: 96−103.
[17] FULEKAR M H, SINGH A, DUTTA D P, ROY M, BALLAL A, TYAGI A K. Ag incorporated nano $BiPO_4$: Sonochemical synthesis, characterization and improved visible light photocatalytic properties [J]. RSC Advances, 2014, 4(20): 10097−10107.
[18] GUAN Mei-li, MA De-kun, HU Sheng-wei, CHEN Yan-jun, HUANG Shao-ming. From hollow olive-shaped $BiVO_4$ to n-p core−shell $BiVO_4$@ Bi_2O_3 microspheres: controlled synthesis and enhanced visible-light-responsive photocatalytic properties [J]. Inorganic Chemistry, 2010, 50(3): 800−805.
[19] LI X Z, LI F B, YANG C L, GE K W. Photocatalytic activity of WO_x−TiO_2 under visible light irradiation [J]. Journal of Photochemistry and Photobiology A: Chemistry, 2001, 141(2): 209−217.
[20] LI F B, LI X Z. Photocatalytic properties of gold/gold ion-modified titanium dioxide for waste water treatment [J]. Applied Catalysis A: General, 2002, 228(1): 15−27.
[21] LI Hui-quan, HONG Wen-shan, CUI Yum-in, HU Xiang-yang, FAN Su-hua, ZHU Liang-jun. Enhancement of the visible light photocatalytic activity of $Cu_2O/BiVO_4$ catalysts synthesized by ultrasonic dispersion method at room temperature [J]. Materials Science and Engineering B, 2014, 181: 1−8.

$MnO_x/BiPO_4$ 异质结光催化剂的光化学合成与增强的光催化活性

李海斌，黄国游，张 健，付圣豪，王腾淦，廖红卫

长沙理工大学 材料科学与工程学院，长沙 400114

摘 要：采用 CTAB 辅助水热法制备棒状单斜相 $BiPO_4$。通过光沉积在 $BiPO_4$ 表面负载 MnO_x 纳米粒子，形成 $MnO_x/BiPO_4$ 异质结。采用 XRD、SEM、TEM、XPS、PL 及 UV-Vis 等手段对样品进行表征。结果表明：当 Mn/Bi 摩尔比控制在较低水平时，MnO_x 纳米粒子牢固附着在 $BiPO_4$ 表面，形成具有有效界面的 $MnO_x/BiPO_4$ 异质结。亚甲基蓝光降解实验结果表明，$MnO_x/BiPO_4$ 异质结相对 $BiPO_4$ 具有更高的光催化活性。这是因为异质结的形成，促进了界面电荷迁移，抑制了光生电子−空穴对的复合，从而获得更高的量子效率。而且 $MnO_x/BiPO_4$ 异质结相对 $BiPO_4$ 在 300~420 nm 范围内具有更高的光吸收能力，这也有利于增强光催化活性。

关键词：$BiPO_4$；光催化；水热法；MnO_x；异质结；光沉积

(Edited by Xiang-qun LI)